Screw dislocation dipoles in niobium: combination of STM observations and atomistic simulations

Joel Bonneville, Christophe Coupeau, Joël Douin, Roman Gröger

Screw dislocation dipoles in niobium: combination of STM observations and atomistic simulations

J Bonneville[1], C Coupeau[1] , J Douin[2] and R Gröger[3]

[1] Institut Pprime, Université de Poitiers/UPR 3346 CNRS/ENSMA, Bat. SP2MI, Site du Futuroscope, 86962 Chasseneuil Cedex, France

[2] CEMES, UPR 8011 CNRS/Université Paul Sabatier de Toulouse, France

[3] Institute of Physics of Materials and CEITEC IPM, Czech Academy of Sciences, Brno-střed, Czech Republic

Abstract

We recently developed an experimental device that allows us to observe the slip traces under stress at the atomic scale. Here, we report experimental results obtained at the latter scale on Nb single crystals making it possible to observe dislocation dipoles (DD), which are evidenced by two slip traces formed by emerging moving dislocations of opposite Burgers vectors ending very close to each other. The geometry and stability of the DD were fully characterized in the framework of linear anisotropic elasticity theory and by atomistic simulations. This allows us to calculate a local opposite stress impeding dislocation motion of the dislocations of the dipole.

Keywords: dislocation dipole, STM, BCC metals

1. Introduction

As mentioned in the obituary published in Scripta (2023) and in Acta (2023), Ladislas Kubin began his scientific career by working on the plastic deformation mechanisms in bcc metals and, more specifically, of Nb single crystals. His last article, published almost forty years later, was also dealing with the plasticity of Nb single crystals as well as with atomic-scale scanning tunneling microscopy (STM) observations of slip traces (Douat *et al* 2019), which clearly demonstrates his passion for this topic throughout a major part of his career. Ladislas has addressed an enormous number of materials subjects in his career, offering a multitude of possible choices for an article. Nevertheless, it seems quite logical to us to dedicate this article as a continuation of his last work. We hope that the present article meets all the requirements that Ladislas would have desired.

The characterization of single crystal slip systems involved in plastic deformation of materials, *i.e.* the Burgers vectors of dislocations and their motion planes, can be achieved using several experimental techniques. Some of them can be macroscopic such as the optical observations of the slip traces (Boas *et al* 1931, Duesbery *et al* 1969) to determine the motion planes and the change in sample shape to determine the Burgers vector (Carrard *et al* 1988). More finer analyses of motion planes can be performed using x-rays (Marichal *et al* 2013) and scanning electron microscopy (Kubin 1971), as well as by transmission electron microscopy (Louchet *et al* 1975), the most informative technique regarding dislocation motion being undoubtedly the *in-situ* deformation experiments (Louchet *et al* 1979, Caillard *et al* 2016). However, when atomic scale resolution is required, these techniques suffer from the lack of resolution which makes them unsuitable. High resolution transmission electron microscopy offers the atomic resolution but it usually requires specific crystallographic orientations which strongly restricts its application field. In this context, STM has proved its capability of imaging the atomic structures of surfaces (Binnig *et al* 1987). It has been, for instance, successfully used to reveal the atomic configurations of dislocation cores emerging on the surface of Au (Wöll *et al* 1989, De la Figera *et al* 1998, Rodriguez *et al* 2002, Engbaek *et al* 2006). *In situ* STM deformation experiments have also been developed which, for technical reasons, are essentially limited to the elastic stage of the investigated materials (Fries *et al* 1994). Because our final goal is to extract significant new information concerning the plastic deformation of various crystalline materials, we have built an experimental device, which combines a deformation setup with STM, allowing us to apply large strains and to follow at increasing strain the surface atomic patterning due to

dislocation movements (Nahas *et al* 2013). The first results obtained on Nb single crystals were published in Douat *et al* (2019). It has been reported that even observed at the atomic scale, the identification of motion planes from slip traces is not straightforward as they follow the crystallographic structure of the surface. This may lead to certain ambiguities, except when the slip traces correspond to pure {011} slip planes. It was also observed, but not reported, slip traces running in opposite directions that ended close to each other. These surface configurations are the signature of dislocation dipoles (DD) within the bulk and will be the subject of the present article.

A DD consists of two dislocations of opposite sign that have parallel lines on different planes separated by a nanometer scale distance (Kroupa 1966). The DD can be formed by various processes, such as formation of sessile jogs on moving dislocations, or by two individual dislocations of opposite Burgers vectors gliding onto two parallel slip planes such as those presented hereafter. This yields a variety of possible configurations whose stability mainly depends on the dislocation characters and their core geometries. Basically, whatever the used linear elasticity frame, *i.e.* isotropic or anisotropic, the interaction force between the two dislocations of the dipole is inversely proportional to their distance r, so that the smaller the r the stronger their interaction. As this interaction force can achieve large values, moving dislocations may trap each other and DD formation can have a significant influence on the mechanical properties of crystals, in particular on hardening when present in large numbers (Hirth and Lothe 1982, and the references therein). Moreover, unlike a single dislocation for which its elastic energy is not theoretically bounded since it grows logarithmically, *i.e.* its stress field decreases as $1/r$, the elastic energy of a DD is finite and decreases much faster as $1/r^2$, which makes DD much more energetically favorable. Therefore, DDs have been the subject of several studies regarding their stabilities and annihilation conditions (Wang 2017), with a special focus on the critical dipole height that is the critical distance between the two glide planes below which the dipole annihilates. Because we report on surface-observed DDs, the measured distances between the two dislocations forming the DD may be different than the critical dipole height. Nevertheless, observations of their stable configurations using STM allow us to characterize the magnitudes of the friction stresses that prevent their annihilations.

The article is organized as follows. First, the experimental details regarding the sample preparation, crystallographic considerations and deformation conditions will be concisely presented, more information been available in Douat *et al* (2019, 2020). Then, detailed descriptions of the experimental results are given and illustrated by a typical STM atomic-scale image of a DD observed after deformation at $T = 293$ K and $\tau a = 35$ MPa. Atomistic simulations, which are required for a rigorous analysis of the experimental results, are presented in appendix A.

The experimental parameters are then compared and discussed with respect to the parameters calculated in the framework of anisotropic linear elasticity given in appendix B. This yields an estimate of the frictional stresses opposing to the motion of screw dislocations for which possible interpretations are offered before concluding.

2. Experiments

2.1 Sample preparation and deformation features

The experimental procedures have already been detailed elsewhere (Douat *et al* 2019, 2020) and are here recalled for the sake of completeness. Nb single crystals were produced by the electron beam floating zone technique, which ensures a low impurity content. There are about 180 ppm substitutional Ta, 25 ppm C, 15 ppm O, less than 5 ppm N and minor traces of other elements. Compression samples of nearly 2 mm x 2 mm in cross section with a gauge length of 6 mm were prepared according to given specifications by Surface Preparation Laboratory (Zaandam, Netherlands). Sample surfaces suitable for atomic scale imaging of slip traces by STM were obtained by successive cycles of Ar sputtering (1 kV and 6 μA for 5 min) and annealing at 1275 K for 2 h under ultra-high vacuum (UHV) environment. Chemical Auger electron analyses were *in situ* performed prior to the straining experiments, highlighting the very low surface contamination levels of oxygen and carbon (Coupeau *et al* 2015).

The samples were deformed under UHV environment in a device specifically designed for *in situ* examinations of surfaces at the atomic-scale by STM (Nahas *et al* 2013). The samples were deformed at three different temperatures, namely 90 K, 200 K and 293 K in strain-control mode, at a strain rate of about 10^{-5} s^{-1}.

To achieve a better resolution, straining was stopped during image data acquisition. The samples were thus allowed to deform under stress relaxation condition until very small strain rates of about 10^{-7}–10^{-8} s^{-1}, ensuring a practically constant applied stress at which image data acquisition was launched. The compression axis was along the $[\bar{1}12]$ crystallographic direction and the observation surfaces were $(1\bar{1}1)$ oriented with misorientations smaller than 0.5° to minimize the density of vicinal steps. Previous studies on Nb (Douat *et al* 2019, 2020) have shown that the observed slip traces left at the observation surface by the emergence of moving dislocations mainly correspond to combinations of {011} and {112} planes associated with a/2[111] and a/2 $[\bar{1}\bar{1}1]$ Burgers vectors. The corresponding slip traces were inclined at an angle of approximately 60° from the compression axis, with an elementary height $h_e = a/2\sqrt{3} = 95$ pm, where $a = 0.330$ nm is the lattice parameter for Nb (Roberge *et al* 1975).

2.2 STM characterization of DD

The slip traces on Nb surfaces observed at the atomic scale by *in situ* STM imaging have already been reported elsewhere (Douat *et al* 2019, 2020). These studies were mainly devoted to the identification of their associated crystallographic planes. In addition, slip traces that ended very close to each other were also repeatedly observed. A typical image of such an event is shown in figure 1. This characteristic STM image was obtained at 293 K under an applied shear stress of $\tau_a = 35$ MPa. The atomic structure of the $Nb(1\bar{1}1)$ surface is clearly distinguishable and exhibits the (2 x 2) reconstruction, as previously reported in the literature (Pantel *et al* 1977, Coupeau *et al* 2015).

The surface exhibits four slip traces (respectively labeled T1 to T4 in figure 1(a)) resulting from moving dislocations in the bulk. The slip traces on the (1-11) surface are lying at approximately 60° from the compression axis, which agrees with our previous studies (Douat et al 2019, 2020). The STM profiles exhibit the height of nearly h~97 pm for each trace, which confirms that they are produced by a single dislocation (figure 1(b)). Two traces (T2 and T3) end in the STM scan area (27 nm x 27nm), the dislocation cores being located at the ending points. The surface contrast of these dislocations results from the out-of-plane component of their Burgers vector. Thus, their reverse contrasts (see rounded arrows in figure 1(a)) indicate that these two dislocations have opposite Burgers vectors. Moreover, measuring the in-plane shift across the slip traces and combining it with the out-of-plane component allows a complete determination of their Burgers vectors. This can be done either directly on the STM image or by more sophisticated methods using the displacement fields deduced from the Fourier transform of the surface image in the error signal mode (Douat 2018). According to our crystallographic conventions, using both their out-of-plane and in-plane components, the Burgers vectors are respectively a/2 [111] for the dislocation with the clockwise rounded arrow and a/2 [-1-1-1] for the dislocation with the anticlockwise rounded arrow, which confirms the dipolar nature of the observed configuration. No evolution of the dislocation positions of the dipole was observed during imaging.

The pertinent geometrical surface parameters used for characterizing the DD are shown in figure 2(a). These are x_s and y_s, the distances between the two emerging points of the dislocations on the surface measured along the [121] and $[\bar{1}01]$ directions, respectively. Note that the [121] direction corresponds to the intersection of the activated slip plane with the free surface, *i.e.* to the slip trace direction. In order to obtain reliable results, ten DD have been experimentally examined under different applied stress levels at three temperatures. The results are reported in table 1. The planes associated with the slip traces of the dislocations forming the dipole, determined using the analysis procedure proposed in Douat *et al* (2019), mainly belong to $(\bar{1}01)$ planes. Therefore, the applied shear stresses τ_a were calculated from the applied stress using a Schmid factor $m = 0.41$ corresponding to the $[111](\bar{1}01)$ slip system. It should be noted that the dipole observed at zero stress and 293 K (line 1 in table 1) has been observed after unloading.

3. Result analyses and discussion

Due to their importance in crystal plasticity, DD have already been the subject of numerous studies both from the theoretical and the experimental points of view; for a concise historical review, see Wang (2017). These studies were essentially devoted to DD annihilation in the fcc crystallographic structure, in particular to the critical distances below which DD will annihilate (Essmann *et al* 1973). Therefore, they were mainly restricted to the

annihilation of edge DD for which dislocation climb is required, and annihilation of dissociated screw DD that requires the overcoming of an energy barrier by cross slip (Rasmussen *et al* 2000). Because cross slip of screw dislocations not pinned by defects/impurities (Andric *et al* 2023) is believed to be easy in the bcc crystalline structure, it is usually considered that DD of screw dislocations will not form (Huang *et al* 1999). As a consequence, for this latter case, such calculations are missing in the literature. Our atomic-scale observations by STM, however, prove that such stable dislocation configurations exist in bcc Nb and likely also in other bcc crystals. In addition, because the two dislocations are immobile during imaging, it can be considered that the dislocations of the dipole are at an equilibrium position.

TEM observations of dislocation microstructures of bcc metals deformed at low temperature reveal that they are predominantly composed of long screw dislocation segments (Louchet and Kubin 1975). We will therefore consider hereafter that the dislocations of the dipoles also have the screw character. STM experiments provide only surface information, which has to be related to the geometric characteristics of the DD deeper in the sample. However, surfaces may have significant influence on the orientation and stability of emerging dislocations. In particular, it is known that, when a dislocation emerges on the surface, image forces bend the dislocation toward it. This has been experimentally verified (Yoffe *et al* 1961, George *et al* 1980). The actual shape of the dislocation can be obtained using atomistic simulations based on physically justified empirical or semi-empirical interaction potentials. Moreover, these simulations are also needed to quantify the effect of the lattice friction stress on the dipole and to determine the angles θ which correspond to stable dipole configurations.
The details of these simulations can be found in appendix A. From figure A1, it is shown that the emergence point of the dislocation on the surface (marked B) is shifted by about $t \sim 7$ nm, with respect to the expected point in the case of a pure screw dislocation (marked A). However, the two dislocations in the dipole have the same screw character in the bulk and thus, for symmetry reasons, a similar effect is expected for both (see the red lines in figure 2(b) showing the DD inside the sample). We argue that combining the experimental parameters (x_s and y_s) as determined by STM and the shift t (obtained from atomistic simulations) allows us to deduce precise positions of the two dislocations inside the sample.

Second, it was shown necessary for our modeling to characterize the DD with respect to the R_v coordinate system (the one linked to the dislocation line; see figures 2(b) and (c)), instead of the one of the surfaces R_s. By simple geometrical considerations, we have:

$$x_v = x_s \sin(19.5^\circ) \sim x_s/3, \tag{1}$$

and

$$y_v = y_s. \tag{2}$$

It follows that, using the measured surface distances x_s and y_s, the distance r between the two dislocations inside the sample is:

$$r = \sqrt{x_v^2 + y_v^2} \sim \sqrt{x_s^2/9 + y_s^2} \tag{3}$$

and the angle θ between the two dislocation lines in the coordinate system R_v (see figure 2(c)):

$$\theta = \arctan\frac{y_v}{x_v} \sim \arctan\frac{3y_s}{x_s} \tag{4}$$

The polar coordinates (r, θ) are given in table 1 for each experimentally observed DD. $\theta = 90^\circ$ corresponds to a dipole with the two dislocations aligned normal to the slip planes (see figure 2(c) for reference).

The equilibrium positions of the screw dislocations in a DD were calculated in the framework of anisotropic linear elasticity. The material anisotropy for the dislocation positions in the dipole is accounted for by the parameter δ (see appendix B). $\delta = 0$ corresponds to the case of an isotropic material and is ranging from $\delta = 0.064$ to $\delta = 0.078$ for $T \in [90\text{–}300\ \text{K}]$ for Nb (Carroll *et al* 1965). As shown in appendix B, the interaction force F_p^i in the $(\bar{1}01)$ plane (per unit length) of an infinite screw dislocation of the dipole acting on the other is given by:

$$F_p^i = -\frac{b^2 \cos\theta(8\delta\cos^4\theta - 10\delta\cos^4\theta + 3\delta - 1)}{2\pi S_{44}\sqrt{1-\delta}\,(1-\delta\cos^2 3\theta)\,r}, \tag{5}$$

with S_{44}, the elastic compliance defined in Appendix B, and $b = a\sqrt{3}/2$, the Burgers vector modulus of the dislocations in the dipole. The temperature dependences of δ and S_{44} have been obtained using the elastic coefficients reported in Caroll *et al* (1965). At 90 K, the elastic coefficients have been estimated by interpolation between 80 K and 100 K. Therefore, as shown in Appendix B, by only considering the interaction force F_p^i, the equilibrium positions of the dislocations in the dipole should correspond to the configuration where the two dislocations are aligned normal to their slip planes, *i.e.* for $\theta = 90^\circ$. This agrees with the atomistic simulations detailed in appendix A, where this equilibrium is either precisely at $\theta = 90^\circ$ (dislocations separated by odd number of planes) or very close to it as shown in figure A2(b) (dislocations separated by even number of planes). It must be noted that F_p^i is always attractive between the two dislocations, except for $\theta = 90^\circ$ for which F_p^i is zero, and that the maximum of F_p^i occurs for all the dipoles at two angles which are respectively smaller or larger than those experimentally observed. For instance, for the dipole 4 reported in table 1, the maxima of F^i corresponds to angles of approximately 45° and 135°. Because the STM experimental observations were performed under load, we also have to account for the effect of the applied force. The role of the applied force is different from that of F_p^i since it contributes to bring closer the two dislocations for $\theta < 90^\circ$ and to push them away for $\theta > 90^\circ$. Therefore, the combination of the interaction force and the applied force lead for the dipole configurations to θ angles always larger than 90°.

However, all the equilibrium angles experimentally observed between the two dislocations forming the DD are ranging between 69° to 81°, whatever the temperature and applied shear stress (see table 1). Therefore, none of them is at the equilibrium configurations that are predicted by balance between the interaction force and the applied force. This clearly indicates that, as expected for screw dislocations in the bcc crystallographic structure, it is necessary to introduce a stress opposing the dislocation movements. Such a local stress on {110} slip planes in Nb, labeled τ_{opp} hereafter, has a minimum value that can be estimated by:

$$\tau_{opp} = \tau_a + \frac{b\cos\theta\,(8\delta\cos^4\theta - 10\delta\cos^2\theta + 3\delta - 1)}{2\pi S_{44}\sqrt{1-\delta}(1-\delta\cos^2 3\theta)r}, \qquad (6)$$

with τ_a, the applied resolved shear stress, as defined in the previous section 2.

τ_{opp} was calculated for each dipole listed in table 1 (except for the one without applied stress at 293 K). It must be noticed that equation (6) should also include the internal stress τ_i resulting from the entire dislocation network. τ_i is usually considered as proportional to $\sqrt{\rho}$, where ρ is the total dislocation density. However, both its value and its sign are difficult to estimate for such a local spatial configuration of DD. By considering the low value of the athermal stress recorded for Nb on the yield stress versus temperature plot, it seems quite reasonable to consider it as negligible. The average values of τ_{opp} for the three temperatures are reported in figure 3. It is seen that τ_{opp}, which significantly decreases from 376 MPa at 90 K to 107 MPa at 293 K, is highly temperature dependent indicating that it must result from a thermally activated process. The applied shear stress for each temperature is indicated in figure 3 by a dashed line. Because the interaction stresses weakly depend on temperature, *i.e.* their temperature dependence arising from those of the elastic coefficients only, the temperature dependence of the τ_{opp} are mainly reflected by the change in the applied stress.

The crucial point we are facing is to understand why the screw dislocations which constitute the dipole experience opposite forces greater than the applied stress at which the plastic deformation occurs. In other words, why the dislocations of the dipole undergo larger friction stresses than those experienced by a single dislocation. This suggests an additional local friction stress that would be reinforced by the interaction force between the two dislocations of the dipole during its formation process. As developed below, the atomistic simulations performed without an applied external stress at 0 K could provide a possible explanation to this question. The existence of the dislocation dipole provides a driving force which tends to bring the two dislocations closer and annihilate. This attraction is opposed by a periodic lattice friction stress which tends to stabilize the two dislocations at a finite distance. In figure 4(a), we use the concept of differential displacement maps (Vitek *et al* 1970) to visualize the core structure of an isolated $a/2[111]$ screw dislocation, and in figure 4(b) the core structures of the $a/2[111]$ and $a/2\ \bar{1}\bar{1}\bar{1}$ screw dislocations forming the dipole configurations with $\theta = 60^\circ$ and 90°. These maps have been obtained by molecular statics relaxation using the same bond order potential (BOP) as described earlier. The calculations were done using an orthogonal simulation cell similar to that used in the second part of appendix A, only with 767 atoms in region 1 and 2065 atoms in region 2. The arrows between atoms are proportional to relative displacements of two neighboring atoms after inserting

the dislocation, projected along the Burgers vector (hereafter called as screw displacements). As shown in figure 4(a), the core of an isolated
$a/2[111]$ screw dislocation spreads symmetrically on three {110} planes in the zone of the Burgers vector. However, when the dipole forms, as shown in figure 4(b), the attractive interaction between the two dislocations results in out-of-glide plane core distortions. At the same time, the dipole with $\theta = 60^\circ$ (left panel in figure 4(b)) shows that the horizontal branches of the two dislocations are extended toward the middle of the figure, which suggests that the dislocations will experience lower frictional stress to move toward the $\theta = 90^\circ$ configuration than the isolated dislocation. This effect is further quantified by the nudged elastic band calculations in appendix A and shown in figure A2(b).

The molecular statics simulations of the dipole of two parallel infinite screw dislocations predict that the stable configuration of the dipole is $\theta = 90^\circ$, which does not agree with the experimental results in table 1, where all dipole angles are smaller than 90°. This suggests that the additional local frictional stress may have its origin in the bending of the dislocation toward the surface as shown in figure A1. As the two dislocations in the dipole change their character from pure screw (in the bulk) toward edge (on the surface), linear elasticity predicts that the stable dipole angle changes from 90° (screw dipole) toward 45° (edge dipole). As the two dislocations move together on parallel planes and experience their attractive force, the surface segments would stop for an angle between 45° and 90°, while the long screw parts of the dislocation tend to move further into the 90° configuration. This motion is, however, opposed by the edge components of the two dislocations, because the90° edge dipole is an energy maximum. Owing to the disagreement of atomistic studies on pure screw dislocations with experiments and considering the qualitative argument above, we believe that the extra local frictional force originates from the non-screw terminating ends of the two dislocations, which hinder the transformation of the dipole into the 90° configuration. It is finally also noted that the slip trace generated at the free surface by the moving dislocation results in an increase of the energy, which may also explain the lower equilibrium angle in the two dislocations of the dipole.

4. Summary

In this article, we presented experimental results obtained during *in situ* deformation of Nb single crystals under STM atomic scale imaging. The reported results were mainly focused on DD clearly identified by the traces, running in opposite directions, left on the surface by each dislocation forming the dipole. Three temperatures were investigated, *i.e.* 293 K, 200 K and 90 K. The experimental observations have been supplemented by atomistic simulations and calculations performed in the framework of anisotropic linear elasticity. The results can be summarized as follows:

- atomic scale imaging of ending slip traces by STM allows a direct determination of the dislocation Burgers vectors,
- atomistic simulations and anisotropic calculations yield very similar, but not exactly equal, dipole configurations if considering only the interaction force between the two dislocations of the dipole,
- none of the dipoles are at the predicted configurations $\theta \geqslant 90^\circ$ considering only the interaction force between the dislocation dipole and the applied stress,
- atomistic simulations show that the interaction force between two opposite screw dislocations forming the dipole in the bulk results in out-of-glide plane core extensions of the screw dislocations composing the dipole, resulting however in a smaller lattice friction stress than the one calculated for the motion of an isolated dislocation,
- the simulations suggest that the experimental measurements cannot be explained solely by the interaction of the long screw parts of the dislocations in the dipole,
- we propose that the origin of the local frictional stress that stabilizes the dipole at $\theta < 90^\circ$ arises from the bending of these dislocations at the surface, where the non-screw segments hinder the glide of long screw arms.

Acknowledgments

The authors are very grateful to B Douat for his permission to use some of the results and figures of his doctorate thesis. J Bonneville and C Coupeau are deeply grateful to Ladislas Kubin for sharing his immense knowledge in dislocation theory, his pertinent advice and his enlightening suggestions during the writing of Douat *et al* (2019). Thanks also to M Drouet for his technical support concerning the Nanoplast UHV experimental set-up.

Appendix A

We have first utilized atomistic simulations in LAMMPS (Thompson *et al* 2022) to determine the shape of the $a/2[111]$ screw dislocation that emerges on the $(1\bar{1}1)$ surface of bcc Nb. The interaction forces between atoms were described using the BOP designed specifically for Nb (Cak *et al* 2014). Several types of surface reconstructions were considered, but only two were found to be in equilibrium. These are the 1 x 1 unreconstructed surface with energy 2.44 J m^{-2} and the 2 x 2 reconstructed surface with energy 2.39 J m^{-2} (for more detail see Coupeau *et al* 2015). The prediction of the stability of the 2 x 2 reconstructed surface agrees with STM measurements, whereas previous DFT studies (Coupeau *et al* 2015) predict an opposite trend (2.40 J m^{-2} for 1 x 1 and 2.42 J m^{-2} for 2 x 2 surface).

In the next step, we have determined the equilibrium shape of the $a/2[111]$ screw dislocation emerging on the 2 x 2 reconstructed $(1\bar{1}1)$ surface of Nb. The simulation box was orthogonal with the x axis parallel to [121], the y axis parallel to $[\bar{1}01]$, and the z axis parallel to $[1\bar{1}1]$. The atoms in the box were separated into two regions. The region 1 (32981 grey atoms in figure A1) comprised atoms close to the boundary of the box in the x and y directions, as well as those in the lower part of the box along the z direction. It represented a boundary layer with the thickness larger than the interaction radius of atoms. The region 2 contained 37 024 atoms inside the simulation cell, including those representing the surface terminating the box in the positive z direction. The size of the simulation cell was determined so that the boundary conditions do not affect the shape of the dislocation. This was achieved by increasing the block size until a sufficiently long straight part of the dislocation was achieved at the bottom of the region 2. The simulation box was first relaxed at 0 K using the FIRE method (Bitzek *et al* 2006) without dislocation by minimizing its potential energy, which results in a small contraction in the direction perpendicular to the $(1\bar{1}1)$ surface. During this calculation, only the atoms in region 2 were allowed to move, while those in region 1 were held fixed. After that, the $a/2[111]$ screw dislocation was introduced by displacing all atoms in the box using the anisotropic linear-elastic strain field of the dislocation as obtained from the Stroh's sextic theory (1962); see also the book of Hirth *et al* (1982). The atoms in region 2 were then allowed to relax into the positions corresponding to the local minimum of potential energy. During this relaxation, only one end of the dislocation is held in the boundary region 1, but the remaining part of the dislocation can change.

The relaxed shape of the dislocation is shown in figure A1, where the blue atoms are those along the dislocation line as identified using the common neighbor analysis (Honeycutt *et al* 1987) implemented in the OVITO code (Stukowski *et al* 2010). It is evident that the interaction of the dislocation with the free surface produces a curvature of the dislocation near the surface so that the dislocation emerges almost perpendicular to the surface. The curved portion of the dislocation is composed of screw segments whose lengths decrease on approaching the surface. Of prime importance is the depth below the surface in which the dislocation attains a pure screw character, which is $h \sim 5$ nm. This has two main consequences. First, we consider that the two dislocations of the dipole have a pure screw character and the influence of the non-screw portions is negligible. Second, the emergent points of the dislocations are shifted by the distance of $t \sim 7$ nm, as shown in figure A1, which must be accounted for when relating the surface and bulk geometries of the dipoles. We have also investigated the minimum distance of the two parallel $(\bar{1}01)$ planes on which the two dislocations can pass each other without annihilation. This was found to be 7 interplanar distances, which is $h_{\min}/a \approx 4.7$ or approx. 1.6 nm in <110> direction. In a further analysis, we have thus determined the variation of the energy of the system as the two dislocations pass each other on parallel planes with separations larger than this threshold. This calculation was done using a modification of the nudged elastic band method (Henkelman *et al* 2000)

developed in Gröger *et al* (2012) which takes into account relaxations of those degrees of freedom that do not directly affect the position of the two dislocations. The simulation block was orthogonal and was again separated into two regions. The boundary region 1 consisted of 977 inactive atoms that represent the boundary conditions, whereas the remaining 3430 atoms in the region 2 with the dislocation were allowed to relax. The size of the simulation cell was carefully tuned so that the boundary conditions do not have any impact on the calculated data.

The transition pathway was discretized by 55 movable images that were initially obtained by interpolating the atomic configurations between the initial ($\theta \approx 61^\circ$) and final ($\theta \approx 90^\circ$) configurations of the dipole shown in figure A2(a) (for simplicity, the angles are calculated by assuming that each dislocation is at the center of mass of its triangular lattice site). The result is shown in figure A2(b) in blue, where the abscissa represents the sum of the displacements of the two dislocations (the dots on the curves correspond to image numbers 0–56) and the ordinate the energy of the dislocation dipole expressed relative to that for the image 0. It is important to emphasize that only one of the two dislocations moves to the next equilibrium lattice site as the energy passes over the local maximum, while the other dislocation stays fixed. Owing to interaction forces between the two dislocations, these local barriers are somewhat smaller than the Peierls barrier of a single dislocation if the dipole contracts. For our choice of h, the relaxation produces the stable dipole at $\theta \approx 88.7^\circ$. As the dislocations are moving toward each other on these parallel planes (θ changes from 60° to 90°), they experience a set of discrete positions corresponding to the minima of the blue curve. These constitute a set of metastable angles for which the dipole is in the state of local equilibrium against the attractive interaction forces that are pulling the two dislocations toward the $\theta \approx 88.7^\circ$ configuration. The last configuration along the pathway is a local maximum, which follows from the choice of the distance between the glide planes of the two dislocations. If the glide plane of the upper dislocation in figure A2(a) was moved up or down by a half of the periodic distance ($a/\sqrt{2}$), the stable positions of the upper dislocation would shift by a half of the period in the horizontal direction ($a/\sqrt{6}$). As a consequence, the equilibrium angles of the dipole would change but no more than about 1°. For comparison, we also plot in figure A2(b) in gray the lattice friction experienced by a single isolated dislocation. The height of the barrier is about 32 meV Å, which is comparable with the DFT value of 35 meV Å^{-1} obtained by Dezerald *et al* (2014).

Appendix B

The applied force per unit length $\vec{F}$ on a dislocation of Burgers vector $\vec{b}$ induced by a stress tensor σ is given in a general way by the Peach–Köhler equation (Peach et al 1950):

$$\vec{F} = (\vec{b}.\bar{\bar{\sigma}}) \times \vec{\xi}, \tag{B1}$$

where $\vec{\xi}$ is a unit vector along the dislocation line, *i.e.* in the present case for screw dislocations $\vec{\xi} // \vec{b}$. The pertinent coordinate system $R_v = (\vec{x}_1, \vec{x}_2, \vec{x}_3)$ linked to the [111] Burgers vector here is: $\vec{x}_1 // [1\bar{2}1]$, $\vec{x}_2 // [\bar{1}01]$ and $\vec{x}_3 // \vec{b} // [\bar{1}\bar{1}\bar{1}]$, as shown in figure 2(c). Assuming that the dislocations of the dipole are straight and parallel and, as characterized by the slip trace analysis, confined to glide in $(\bar{1}01)$ planes, the relevant interaction force is according to equation (B1)

$$F_{\vec{x}_1} = -b\,\sigma_{23}, \tag{B2}$$

where σ_{23} is the stress component of the dislocation of Burgers vector $\vec{b}$ at the origin of the coordinate system acting on the dislocation of Burgers vector $-\vec{b}$ located at a position (r,θ) (see figure 2(c)). Analytical expressions of the stress tensor components about a dislocation are usually not available for non-specific orientations in the framework of anisotropic elasticity. However, the expression of σ_{23} can be calculated analytically here because $\vec{X3} \parallel [111]$ is a three-fold axis and $\vec{X2} \parallel [\bar{1}01]$ is a two-fold axis, for example following the work of Steeds (1973):

$$\sigma_{23} = \frac{b(\cos\theta - \delta\cos 2\theta\cos 3\theta)}{2\pi\, r\, S_{44}\sqrt{1-\delta}(1-\delta\cos^2 3\theta)}, \tag{B3}$$

with

$$\delta = \frac{S_{15}^2}{S_{11}S_{44}}, \tag{B4}$$

where the S_{15}, S_{11} and S_{44} compliances are expressed in the R_v coordinate system by:

$$S_{15} = \frac{A-1}{3\sqrt{2}C_{44}}, \tag{B5}$$

$$S_{44} = \frac{1+2A}{3C_{44}}, \tag{B6}$$

and

$$S_{11} = \frac{1}{12}\left(\frac{2+A}{C_{44}} + \frac{9A}{3AC_{12} + C_{44}(2+A)}\right). \tag{B7}$$

In these expressions, the C_{ij} are expressed in the coordinate system R_c defined by {[100], [010], [001]} and A is the Zener anisotropy ratio given by:

$$A = \frac{2C_{44}}{C_{11}-C_{12}}. \tag{B8}$$

Using equations (B4)–(B7), the δ ratio can be rewritten as:

$$\delta = \frac{2(A-1)^2(3AC_{12} + C_{44}(2+A))}{(1+2A)(3AC_{12}(2+A) + C_{44}(4+A(13+A))}. \tag{B9}$$

The equilibrium positions of the dislocations of the dipole resulting from their elastic interaction only, *i.e.* in the absence of any other stresses such as applied or internal stresses, are obtained by solving:

$$F_{\vec{x}_1} = -b\,\sigma_{23} == \frac{b^2(\cos\theta - \delta\cos2\theta\cos3\theta)}{2\pi\, r\, S_{44}\sqrt{1-\delta}(1-\delta\cos^2 3\theta)} = 0, \tag{B10}$$

that is

$$\cos\theta - \delta\cos2\theta\cos3\theta = 0, \tag{B11}$$

taking care that the roots obtained do not also cancel the denominator of the equation (B10). Equation (B11) can be rewritten in a more convenient form using the cosine double angle formula: $\cos2\theta = 2\cos^2\theta - 1$, and $\cos3\theta = 4\cos^3\theta - 3\cos\theta$, yielding to:

$$\cos\theta(8\delta\cos^4\theta - 10\delta\cos^2\theta + 3\delta - 1) = 0. \tag{B12}$$

The equilibrium positions of the two dislocations of the dipole are thus given by

$$\cos\theta = 0 \tag{B13}$$

and

$$\cos^2\theta = \frac{5 \pm \sqrt{1+\frac{8}{\delta}}}{8}. \tag{B14}$$

Roots of (B14) are only acceptable if the right-hand side is in between 1 and 0, which imposes for the plus sign $\delta \geqslant 1$ while for the minus sign $\delta \geqslant 1/3$. Therefore, in the case of Nb, for which δ is ranging between 0.064 and 0.078 for the involved temperatures, the unique solution in the frame of linear anisotropy elasticity is $\cos\theta = 0$, that is, likewise in the isotropy case, $\theta = 90^\circ$; the two dislocations are consequently expected to be aligned normal to their slip planes at their equilibrium positions.

References

Acta: Obituary Ladislas Kubin 2023 *Acta Mater.* **246** 118690 Andric P, Restrepo S and Maresca F 2023 *Acta Mater.* **243** 118500 Binnig G and Rohrer H 1987 *Rev. Mod. Phys.* **59** 615–25
Bitzek E, Koskinen P, Gähler F, Moseler M and Gumbsch P 2006 *Phys. Rev. Lett.* **97** 170201 Boas W and Schmid E 1931 *Z. Phys.* **71** 703–14
Caillard D 2016 *Acta Mater.* **112** 273–83W
Cak M, Hammerschmidt T, Rogal J, Vitek V and Drautz R 2014 *J. Phys.: Condens. Matter* **26** 195501 Carrard M and Martin J L 1988 *Phil. Mag.* A **56** 391–405
Carroll K J 1965 *J. Appl. Phys.* **36** 3689–90
Coupeau C, Durinck J, Drouet M, Douat B, Bonneville J, Colin J and Grilhe J 2015 *Surf. Sci.* **632** 60–63 de la Figuera J, González M A, García-Martínez R, Rojo J M, Hernán O S, Vázquez de Parga A L and Miranda R 1998 *Phys. Rev.* B **58** 1169–72
Dezerald L, Ventelon L, Clouet E, Denoual C, Rodney D and Willaime F 2014 *Phys. Rev.* B **89** 24104 Douat B 2018 *PhD Thesis* Université de Poitiers, Poitiers
Douat B, Bonneville J, Drouet M, Vernisse L and Coupeau C 2020 *Scr. Mater.* **183** 81–85
Douat B, Coupeau C, Bonneville J, Drouet M, Vernisse L and Kubin L P 2019 *Scri. Mater.* **162** 292–5
Duesbery M S and Foxall R A 1969 *Phil. Mag.* **20** 719–51
Engbæk J, Schiøtz J, Dahl-Madsen B and Horch S 2006 *Phys. Rev.* B **74** 195434 Essmann U and Rapp M 1973 *Acta Metall.* **21** 1305–17
Fries T, Oster K and Wandelt K 1994 *Acta Metall. Mater.* **42** 3129–36 George A and Champier G 1980 *Scr. Mater.* **14** 399–403
Gröger R and Vitek V 2012 *Model. Simul. Mater. Sci. Eng.* **20** 035019 Henkelman G and Jónsson H 2000 *J. Chem. Phys.* **113** 9978–85 Hirth J P and Lothe J 1982 *Theory of Dislocations* (Wiley) Honeycutt J D and Andersen H C 1987 *J. Phys. Chem.* **91** 4950–63
Huang H, Ghoniem N, Diaz de la Rubia T, Rhee M, Zbib H and Hirth J 1999 *J. Eng. Mater. Technol.* **121** 143–50
Kroupa F 1966 *J. Phys. C3* **27** 154–67
Kubin L P 1971 *Thèse de Doctorat* vol 854 Université Paris-Sud Orsay Louchet F and Kubin L P 1975 *Acta Metall.* **23** 17–21
Louchet F, Kubin L P and Vesely D 1979 *Phil. Mag. A* **39** 433–54
Marichal C, Van Swygenhoven H, Van Petegem S and Borca C 2013 *Sci. Rep.* **3** 2547
Nahas Y, Berneau F, Bonneville J, Coupeau C, Drouet M, Lamongie B, Marteau M, Michel J, Tanguy P and Tromas C 2013 *Rev. Sci. Instrum.* **84** 105117
Pantel R, Bujor M and Bardolle J 1977 *Surf. Sci.* **62** 589–609
Peach M and Koehler J S 1950 *Phys. Rev.* **80** 436–9
Rasmussen T, Vegge T, Leffers T, Pedersen O B and Jacobsen K W 2000 *Phil. Mag.* A **80** 1273–90 Roberge R 1975 *J. Less-Common Met.* **40** 161–4
Rodriguez de la Fuente O, Zimmerman J A, González M A, de la Figuera J, Hamilton J C, Wu Pai W and Rojo J M 2002 *Phys. Rev. Lett.* **88** 036101
Scripta: Obituary Ladislas Kubin 2023 *Scr. Mater.* **277** 115298
Steeds J W 1973 *Introduction to Anisotropic Elastic Theory of Dislocations* (Clarendon) Stroh A N 1962 *J. Math. Phys.* **41** 77–103
Stukowski A 2010 *Model. Simul. Mater. Sci. Eng.* **18** 015012 Thompson A P *et al* 2022 *Comput. Phys. Commun.* **271** 10817 Vitek V, Perrin R C and Bowen D K 1970 *Phil. Mag.* **21** 1049–73 Wang H 2017 *Mater. Sci.* **4** 1231–9
Wöll C, Chiang S, Wilson R J and Lippel P H 1989 *Phys. Rev.* B **39** 7988–91 Yoffe E H 1961 *Phil. Mag.* **69** 1147–55

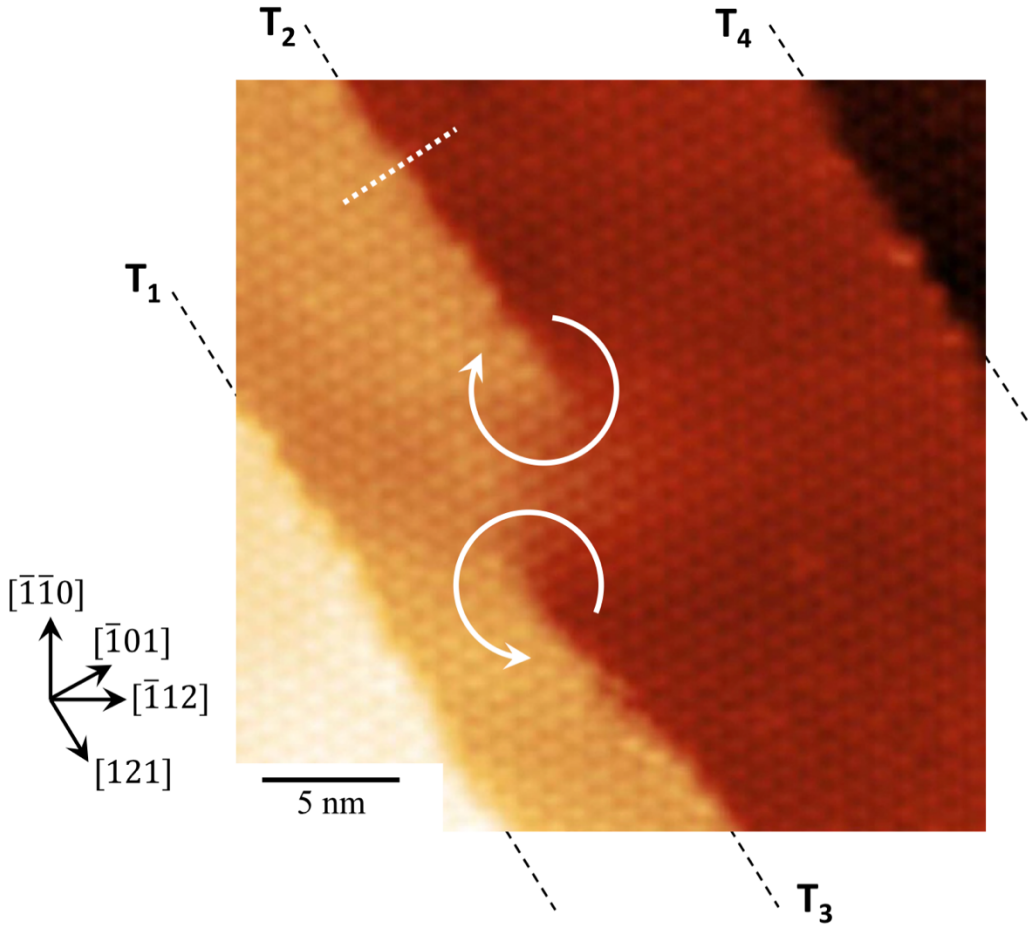

Figure 1: Nb single crystals deformed at T=293 K by compression along the [$\bar{1}$12] direction (a) Typical atomic-scale STM image of a dislocation dipole observed on the Nb (1$\bar{1}$1) surface under an applied shear stress of τ=35 MPa. The white clockwise and anticlockwise rounded arrows indicate respectively the upward and downward directions of the surface steps due to the out-of-plane component of the dislocation Burgers vectors. The slip traces are labelled T_i, for i=1 to 4. (b) Profile associated with T_2 (from the white dotted line in (a)).

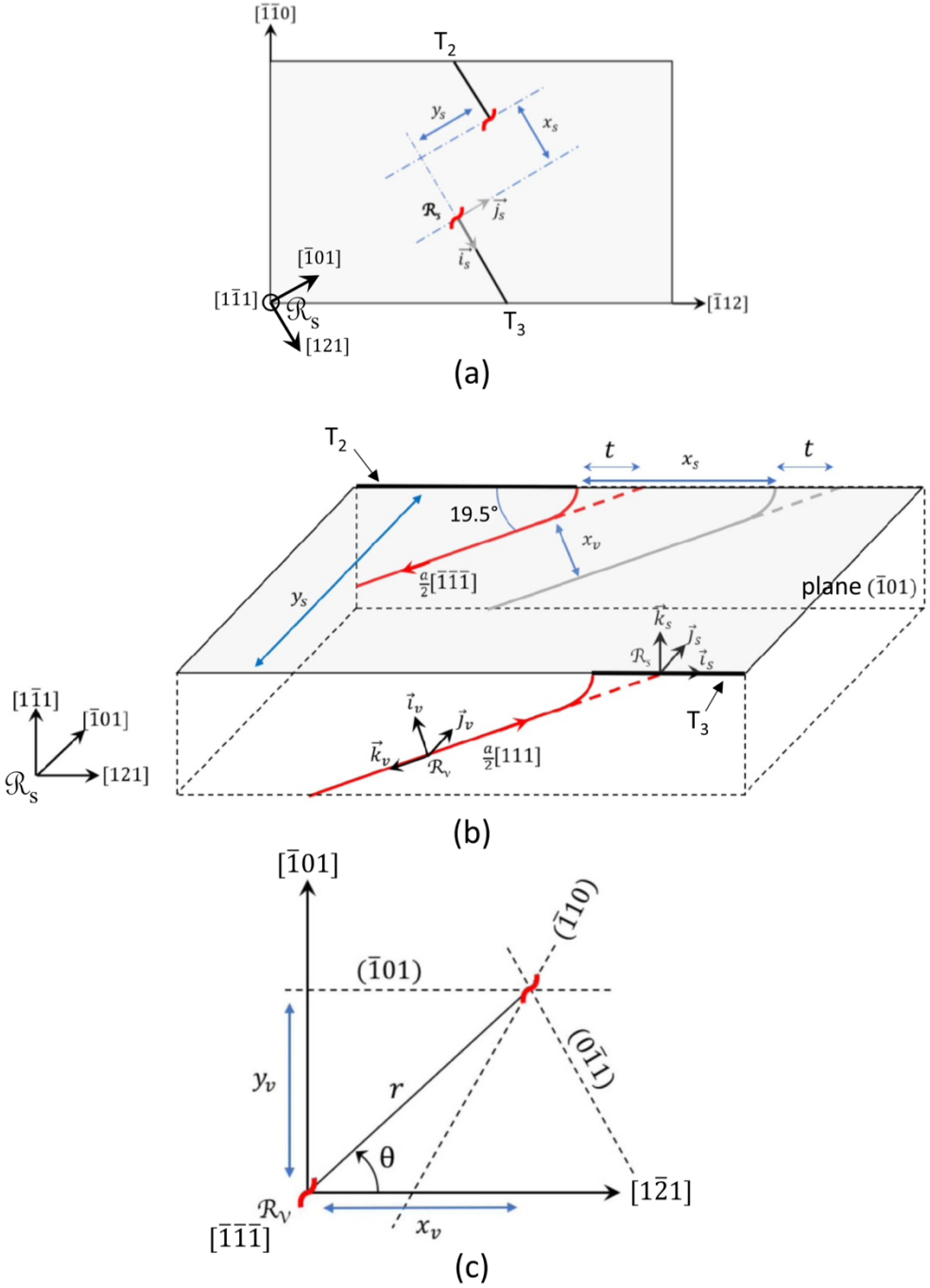

Figure 2: Schematic representations of the dislocation dipole and associated pertinent parameters: (a) Top view of the sample surface (b) Three dimensional bulk view of the sample (c) End-on view of the screw dislocation lines of the dipole.

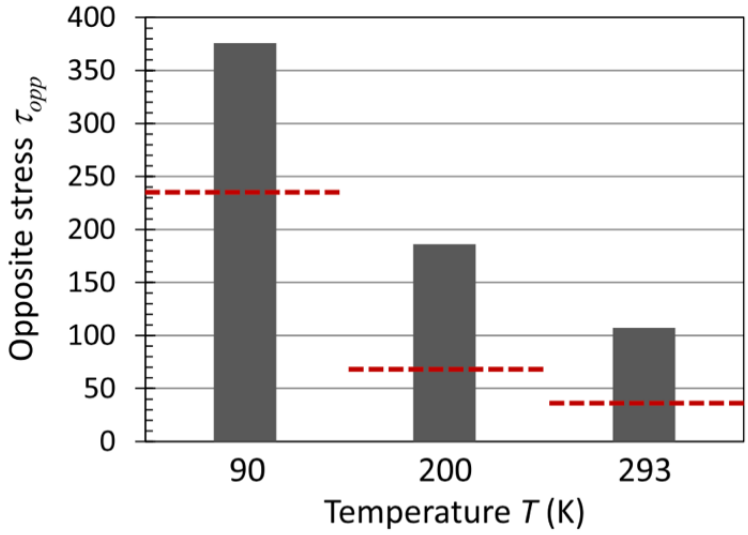

Figure 3: Opposite stresses τ_{opp} calculated for the nine dipoles experimentally observed as a function of temperature. The horizontal lines indicate the levels of the applied shear stresses τ_a.

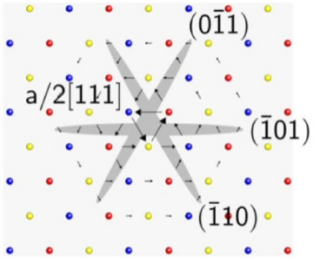

(a)

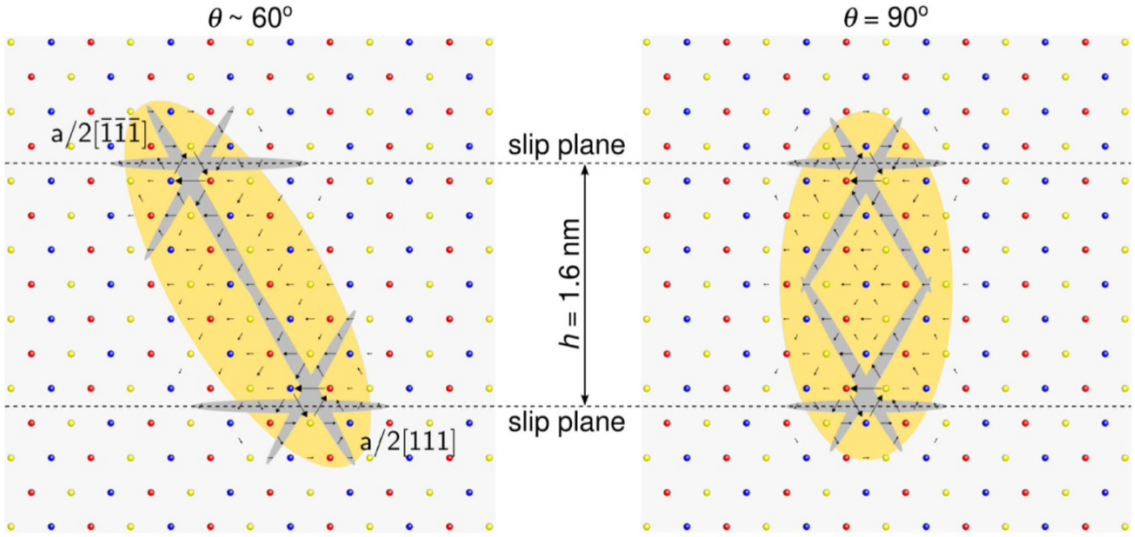

Figure 4. Transformation of core structures by attractive interactions between the two screw dislocations in the dipole for the separation of slip planes h = 1.6 nm. (a) Three- fold symmetric core of an isolated a/2[111] screw dislocation. (b) Core structures of the a/2[111] and a/2[-1-1-1] screw dislocations in two dipole configurations. In all figures, gray ovals represent core spreadings on the three {110} planes (only the arrows above certain size are plotted to visualize the largest bond distortions). In (b) and (c), the major bond distortions are not concentrated in a single plane, but they form bands between the two dislocations that are highlighted by orange ovals.

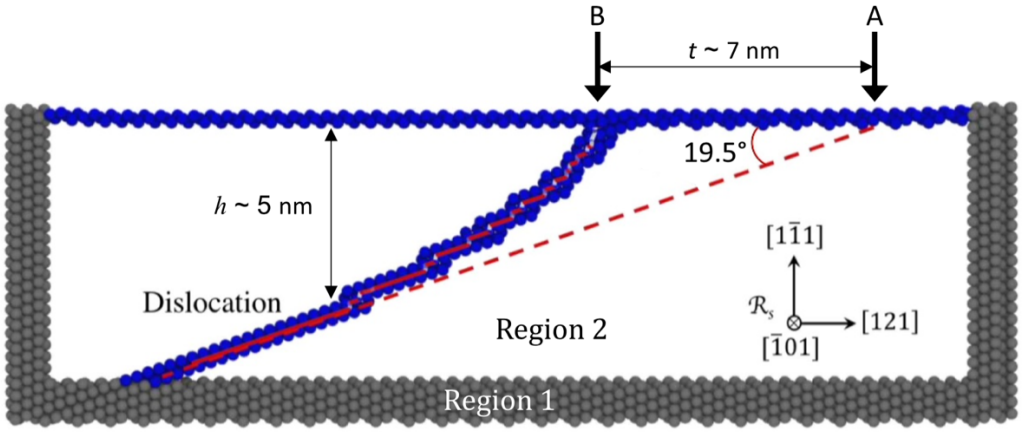

Figure A1: Atomistic calculation of the shape of $a/2[111]$ screw dislocation emerging on the $(1\bar{1}1)$ surface of Nb. The red dashed line illustrates the shape of the dislocation before relaxation.

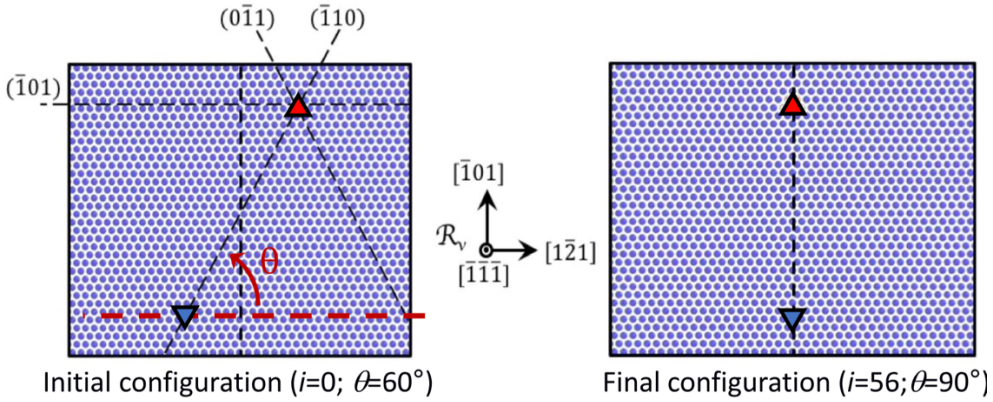

(a)

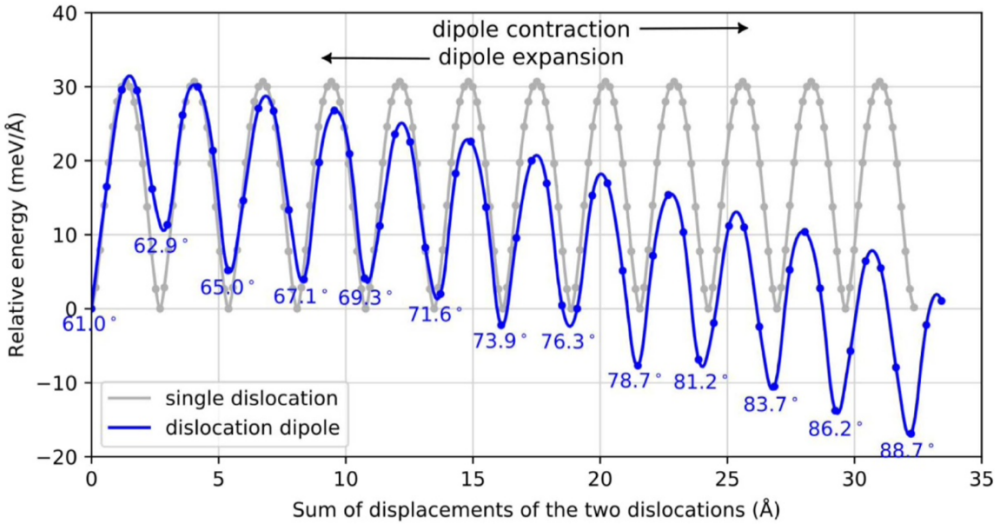

(b)

Figure A2: (a) Initial and final configuration of the dipole. (b) Profile of the relative energy of the system as the two opposite straight dislocations pass each other on parallel $(\bar{1}01)$ planes (blue curve). In this case, the separation of the two planes is 6.07 nm, which is the mean value obtained from STM measurements. The gray curve represents the lattice friction potential of a single dislocation